Cognate antigen directs CD8+ T cell migration to vascularized transplants

Jeffrey M. Walch,[1,2] Qiang Zeng,[1,3] Qi Li,[1,3] Martin H. Oberbarnscheidt,[1,3] Rosemary A. Hoffman,[1,3,4] Amanda L. Williams,[1,3] David M. Rothstein,[1,3,4,5] Warren D. Shlomchik,[6] Jiyun V. Kim,[1,3,4] Geoffrey Camirand,[1,3] and Fadi G. Lakkis[1,3,4,5]

[1]Thomas E. Starzl Transplantation Institute, [2]Immunology Graduate Program, [3]Department of Surgery, [4]Department of Immunology, and [5]Department of Medicine, University of Pittsburgh School of Medicine, Pittsburgh, Pennsylvania, USA.
[6]Departments of Medicine and Immunobiology, Yale University School of Medicine, New Haven, Connecticut, USA.

The migration of effector or memory T cells to the graft is a critical event in the rejection of transplanted organs. The prevailing view is that the key steps involved in T cell migration — integrin-mediated firm adhesion followed by transendothelial migration — are dependent on the activation of $G\alpha_i$-coupled chemokine receptors on T cells. In contrast to this view, we demonstrated in vivo that cognate antigen was necessary for the firm adhesion and transendothelial migration of $CD8^+$ effector T cells specific to graft antigens and that both steps occurred independent of $G\alpha_i$ signaling. Presentation of cognate antigen by either graft endothelial cells or bone marrow–derived APCs that extend into the capillary lumen was sufficient for T cell migration. The adhesion and transmigration of antigen-nonspecific (bystander) effector T cells, on the other hand, remained dependent on $G\alpha_i$, but required the presence of antigen-specific effector T cells. These findings underscore the primary role of cognate antigen presented by either endothelial cells or bone marrow–derived APCs in the migration of T cells across endothelial barriers and have important implications for the prevention and treatment of graft rejection.

Introduction

Allograft rejection is caused by both naive and memory T cells (1). Naive T cells encounter alloantigens in secondary lymphoid tissues, where they differentiate into effector T cells, which in turn migrate to and reject the graft (2). Memory T cells, in contrast, can initiate rejection by directly homing to the graft itself (3–5). The prevailing view is that effector and memory T cell migration to vascularized organ transplants follows the classical leukocyte migration paradigm (6). According to this paradigm, chemokines displayed on the inflamed endothelium engage $G\alpha_i$-coupled chemokine receptors on rolling T cells and trigger their firm adhesion and transmigration via integrin-dependent mechanisms (7). Although blocking integrins has been shown to reduce T cell infiltration and delay graft rejection (8, 9), targeting individual or multiple chemokine receptors has had modest or no effects (10–12). This prompted us to reexamine the role of $G\alpha_i$-coupled chemokine receptors in the migration of effector and memory T cells to vascularized organ transplants. Using mouse models of heart and kidney transplantation and intravital high-resolution microscopy, we established that T cell firm adhesion and transmigration across the graft endothelium was primarily driven by cognate antigen, not by $G\alpha_i$-dependent chemokine receptor signaling. Importantly, we demonstrated that the antigen presentation step required for T cell migration was not restricted to endothelial cells, but was also carried out by bone marrow–derived APCs in the graft.

Results

To investigate whether $G\alpha_i$-dependent chemokine receptor signaling in T cells is required for their migration to vascularized organ grafts, we transplanted BALB/c (H-2D) heart allografts into B6 (H-2B) mice and 2 days later cotransferred pertussis toxin–treated (PTx-treated) and untreated $CD4^+$ and $CD8^+$ memory or effector ($CD44^{hi}$) T cells from B6 mice immunized with BALB/c splenocytes. PTx irreversibly blocks $G\alpha_i$ function, thereby inhibiting chemokine-dependent T cell migration (13, 14). Grafts were removed 1, 3, and 6 days after cell transfer, and the transferred $CD8^+$ T cells were identified by flow cytometry using congenic markers. Comparable numbers of PTx-treated and untreated $CD8^+$ memory T cells were present in the grafts on days 1, 3, and 6 after transfer, and the 2 cell populations proliferated equally, progressing from no division on day 1 to greater than 8 divisions by day 6 (Figure 1A). Significantly diminished migration of PTx-treated T cells to the lymph nodes, a process known to be $G\alpha_i$ dependent (15), confirmed that $G\alpha_i$ was blocked in these cells (Figure 1B). Results similar to those in Figure 1A were obtained when memory T cells were transferred to mice lacking secondary lymphoid tissues (splenectomized *aly/aly* mice; Figure 1C), which indicates that PTx-treated $CD8^+$ memory T cells migrate to the grafts without first proliferating in secondary lymphoid tissues. Likewise, equal numbers of PTx-treated and untreated $CD8^+$ memory T cells infiltrated allografts allowed to heal for 50 days in splenectomized *aly/aly* recipients (Figure 1D), which suggests that acute graft inflammation is not a prerequisite for T cell migration. Similar to memory T cells, $CD8^+$ effector T cells migrated to the grafts independent of $G\alpha_i$ signaling, whereas neither naive ($CD44^{lo}$) nor natural (preexisting) memory T cells transferred from nonimmunized mice were detected in significant numbers in the grafts (Figure 1E). Using splenectomized *aly/aly* recipients, in which allograft rejection is dependent on the transfer of effector or memory T cells (2, 3), we observed that PTx-treated memory T cells caused acute rejection of heart allografts, albeit with a short (but not significant) delay, compared with their untreated counterparts (Figure 1F). These results indicate

Conflict of interest: The authors have declared that no conflict of interest exists.
Citation for this article: *J Clin Invest.* 2013;123(6):2663–2671. doi:10.1172/JCI66722.

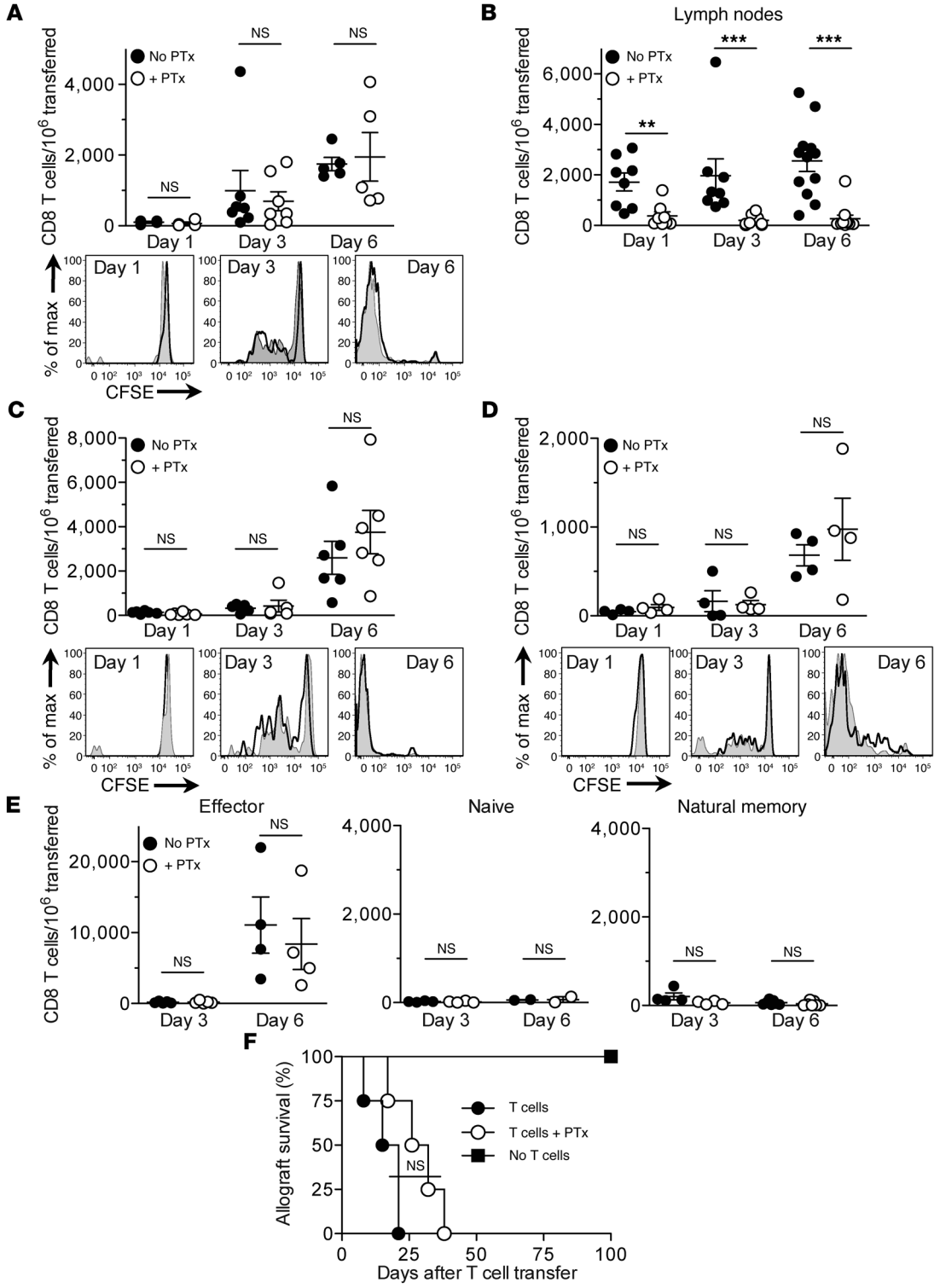

Figure 1

$G\alpha_i$-independent migration of memory and effector T cells to heart allografts. PTx-treated and untreated T cells were cotransferred to heart allograft recipients 2 days after transplantation, except where indicated. (**A** and **B**) Enumeration of transferred memory CD8$^+$ T cells in the grafts (**A**) and lymph nodes (**B**) of B6 recipients. T cell proliferation is shown in the CFSE histograms. (**C** and **D**) Enumeration and proliferation of transferred memory CD8$^+$ T cells in splenectomized *aly*/*aly* recipient grafts. Memory T cells were transferred either 2 days (**C**) or 50 days (**D**) after transplantation. (**E**) Enumeration of effector, naive, and natural memory CD8$^+$ T cells in B6 recipient grafts. (**F**) Heart allograft survival in splenectomized *aly*/*aly* recipients that received either PTx-treated (n = 4) or untreated (n = 4) memory T cells. Results are mean ± SEM. $^{**}P < 0.01$; $^{***}P < 0.001$.

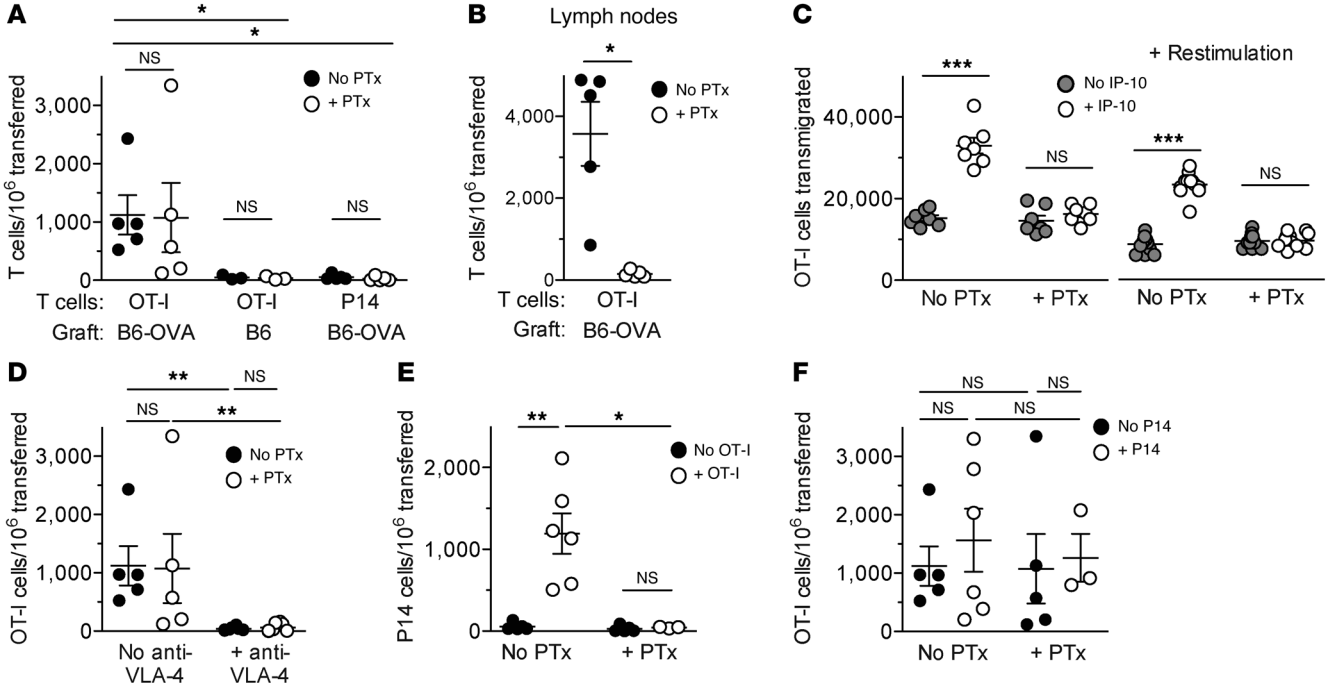

Figure 2

Antigen-dependent migration of effector T cells to heart grafts. (**A** and **B**) PTx-treated and untreated OT-I or P14 effector T cells were cotransferred to heart graft recipients 2 days after transplantation. Transferred cells were enumerated in the grafts (**A**) and lymph nodes (**B**) 3 days after transfer. (**C**) In vitro migration of PTx-treated and untreated OT-I effector T cells in response to IP-10 before and 6 hours after restimulation with cognate antigen. (**D**–**F**) Effector T cells were transferred 2 days after transplantation, and grafts were analyzed 3 days after cell transfer. (**D**) Effect of blocking VLA-4 on the migration of PTx-treated and untreated OT-I effector T cells to B6-OVA heart grafts. (**E**) Migration of P14 effector T cells to B6-OVA heart grafts in the presence or absence of cotransferred OT-I effector T cells and PTx. (**F**) Migration of OT-I effector T cells to B6-OVA heart grafts in the presence or absence of cotransferred P14 effector T cells and PTx. Control groups in **D** (No anti–VLA-4) and **F** (No P14) are taken from the first experimental group in **A**. Control group in **E** (No OT-I) is taken from the third experimental group in **A**. Results are mean ± SEM. $^*P < 0.05$; $^{**}P < 0.01$; $^{***}P < 0.001$.

that, contrary to the prevailing view, $G\alpha_i$-dependent chemokine receptor signaling is not necessary for the migration of effector and memory T cells to vascularized organ transplants.

An alternative mechanism that could govern effector or memory T cell migration and accumulation in the tissues is interaction of the TCR with cognate antigen presented by the endothelium or tissue antigen APCs (16–20). Similar to chemokine receptors, the TCR triggers inside-out signaling that changes the conformation of integrins (namely, LFA-1 and VLA-4) from a low-affinity to a high-affinity ligand-binding state (21–23). Unlike chemokine receptors, however, inside-out signaling via the TCR is independent of $G\alpha_i$ (23, 24). Since we observed that blocking $G\alpha_i$ did not impede the migration of effector or memory T cells to the grafted tissue, we asked whether TCR engagement by cognate antigen drives the migration process. To test this possibility, we transplanted B6-OVA transgenic hearts, which express the non–self-antigen OVA, or syngeneic B6 hearts, which do not express OVA, into B6 recipients and then cotransferred PTx-treated and untreated TCR-transgenic OT-I or P14 $CD8^+$ effector T cells. All T cell transfers were performed 2 days after heart transplantation. Since OVA is recognized by the OT-I but not the P14 TCR, this model allowed us to dissect the requirements for the migration of antigen-specific (OT-I) and antigen-nonspecific (P14) T cells. On day 3 after cell transfer, both PTx-treated and untreated OT-I effector cells were present in B6-OVA grafts in comparable numbers and had proliferated equally (Figure 2A and data not shown). In contrast, OT-I cells did not migrate to B6 grafts, and neither PTx-treated nor untreated P14 effector cells (which do not recognize OVA) migrated to B6-OVA grafts (Figure 2A). PTx-treated OT-I cells did not home to lymph nodes in these experiments (Figure 2B), which indicates that $G\alpha_i$ was adequately blocked. Moreover, PTx-treated OT-I effector cells did not migrate in response to a chemokine gradient in vitro, either before or after restimulation with antigenic peptide (Figure 2C), further confirming irreversible inhibition of $G\alpha_i$ function in these cells. Anti–VLA-4 antibodies blocked the migration of PTx-treated OT-I effector cells to the graft (Figure 2D), which indicated that integrin activation, occurring via a $G\alpha_i$-independent pathway, was still required for effector T cell migration. These findings suggest that cognate antigen recognition is necessary for integrin-dependent migration of antigen-specific effector T cells to the graft, while $G\alpha_i$ signaling is not required.

To study the requirements for the migration of antigen-nonspecific (bystander) T cells, we cotransferred P14 and OT-I effector cells with or without PTx treatment to recipients of B6-OVA grafts. P14 cells migrated to the graft only when antigen-specific OT-I cells were present, and only P14 migration was inhibited when both cell populations were treated with PTx (Figure 2E). In contrast, the migration of OT-I cells was independent of both P14 cells and $G\alpha_i$ signaling (Figure 2F). Therefore, migration of antigen-nonspecific (bystander) T cells is dependent on both antigen-specific effector T cells and $G\alpha_i$.

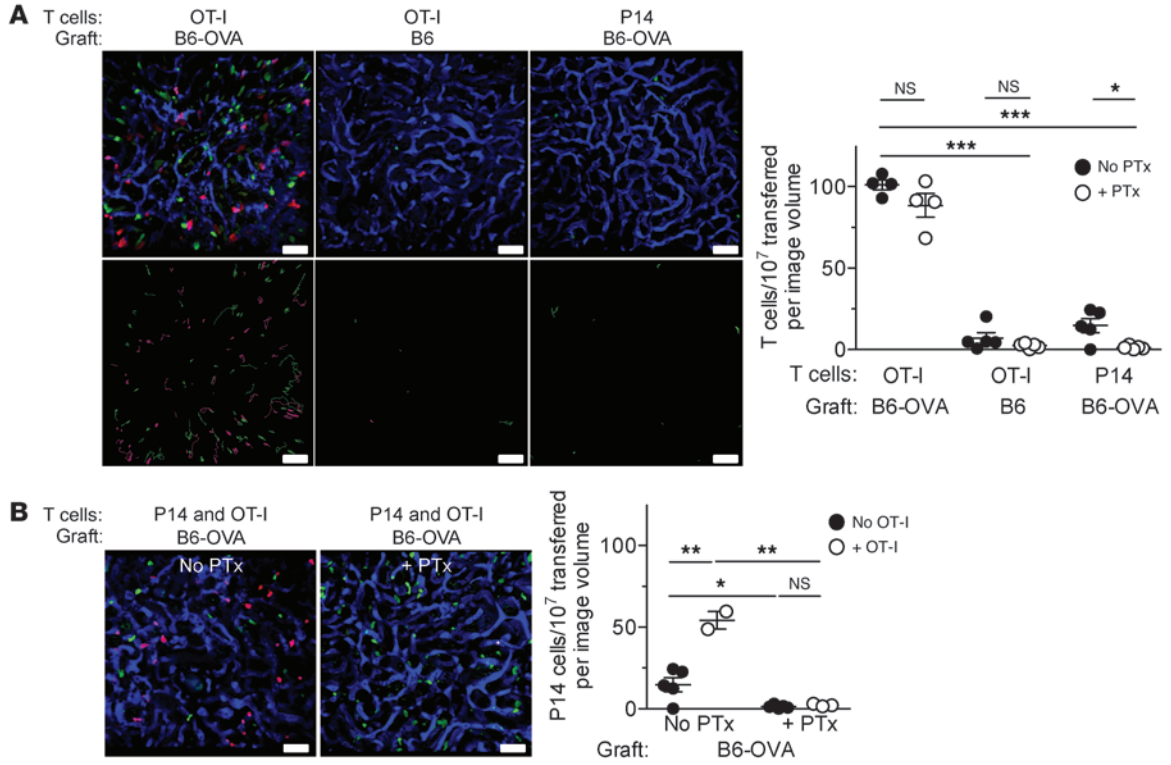

Figure 3

Imaging of effector T cells in kidney grafts by 2-photon intravital microscopy. OT-I and P14 effector T cells were transferred to kidney graft recipients 2 days after transplantation. Grafts were imaged 24 hours after cell transfer. *z* stacks (0.45 × 0.45 × 0.03 mm) were obtained at 30-second intervals. (**A**) Visualization and enumeration of PTx-treated and untreated OT-I and P14 cells arrested in B6-OVA or B6 kidney grafts (*n* = 4–5 videos/group, 2 independent experiments). Volume-rendered representative time point images (top) show arrested PTx-treated (red) and untreated (green) cells in each of the experimental groups; blood vessels are labeled in blue. 30-minute time projections (bottom) depict PTx-treated (red) and untreated (green) cell tracks. (**B**) Volume-rendered representative time point images of B6-OVA grafts after cotransfer of P14 (red) and OT-I (green) cells treated or not with PTx; blood vessels are labeled in blue. Enumeration of P14 cells arrested in B6-OVA kidney grafts in the presence or absence of OT-I cells and PTx is also shown (*n* = 2–5 videos/group, 2 independent experiments). Results are mean ± SEM. $^*P < 0.05$; $^{**}P < 0.01$; $^{***}P < 0.001$. Scale bars: 50 μm.

To investigate the roles of cognate antigen and $G\alpha_i$ in the transmigration of effector T cells across the graft endothelium, we performed real-time, 2-photon intravital imaging of mouse kidney transplants, a procedure previously established in our laboratory (25). Unlike the flow cytometry approach used in Figure 2, intravital microscopy permitted the direct visualization and enumeration of T cells early after transfer, prior to their proliferation in the graft or secondary lymphoid tissues. It also allowed us to determine whether they had firmly adhered to the capillary wall or transmigrated, as well as to calculate their motility parameters. PTx-treated and untreated antigen-specific (OT-I) or bystander (P14) effectors were transferred into B6 recipients of either B6-OVA or B6 kidney grafts 2 days after transplantation, and the grafts were imaged 24 hours later. The number of OT-I and P14 cells present in 30-second-long *z* stacks (i.e., cells per image volume) was enumerated at multiple representative time points and in multiple tissue locations. As shown in Figure 3A and Supplemental Videos 1 and 2 (supplemental material available online with this article; doi:10.1172/JCI66722DS1), OT-I cells migrated to B6-OVA but not B6 kidney grafts, and migration was not inhibited by PTx. In contrast, the migration of antigen-nonspecific (P14) T cells to B6-OVA grafts was considerably less than that of OT-I cells (15 ± 4.3 vs. 101 ± 3 cells per image volume; $P < 0.001$) and was inhibited by PTx (Figure 3A and Supplemental Video 3). These results confirmed the primary role of cognate antigen in effector T cell migration to organ transplants. Similar to the heart graft data in Figure 2E, substantial migration of antigen-nonspecific (P14) T cells to kidney grafts was observed only when cotransferred with antigen-specific (OT-I) cells and was completely inhibited by PTx (Figure 3B).

In order to determine the location of T cells in the graft, we tracked OT-I and P14 cells for more than 2 minutes and ascertained whether they were arrested inside the capillaries or had transmigrated to the extracapillary space. Approximately half the OT-I cells were firmly adhered inside the capillary lumina, while a similar proportion had transmigrated (Figure 4, A and B). Pretreatment with PTx did not reduce the number of either firmly adhered or transmigrated OT-I cells, but completely inhibited the adhesion and transmigration of P14 T cells (Figure 4, A and B). A PTx-treated OT-I cell tracked transmigrating across the capillary wall of a B6-OVA graft is shown in Figure 4C. Motility analysis confirmed that the majority of PTx-treated and untreated OT-I cells and untreated P14 cells enumerated in Figure 3A had arrested in the graft, as judged by their low velocities, short

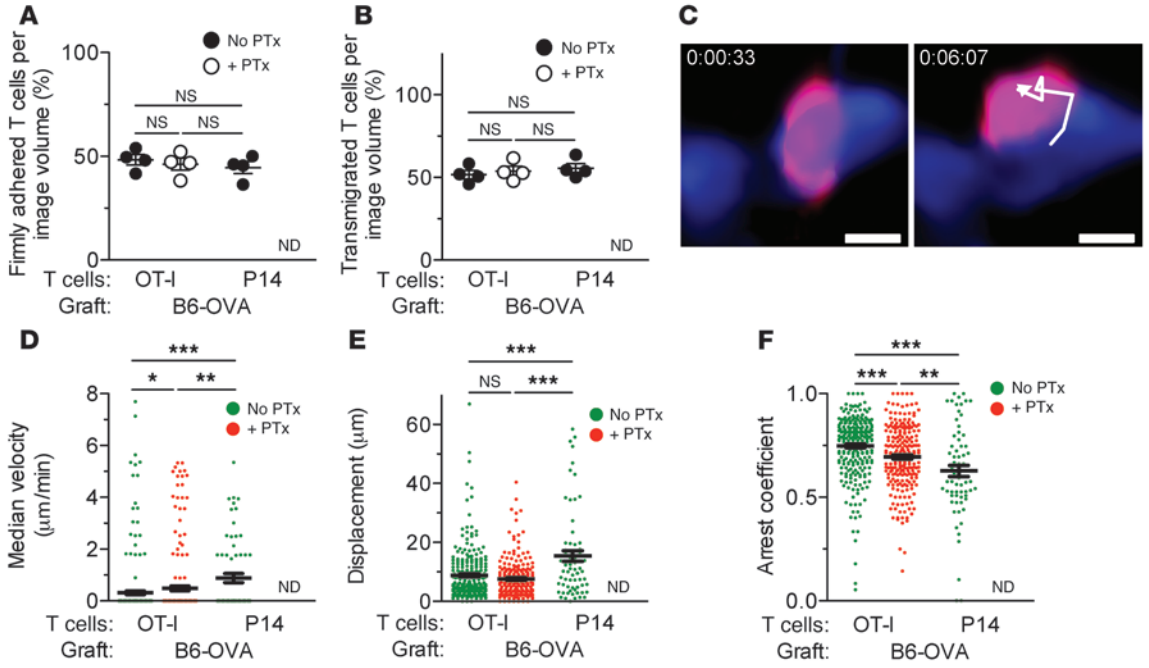

Figure 4

Characterization of effector T cell migration in kidney grafts by 2-photon intravital microscopy. OT-I and P14 effector T cells were imaged as described in Figure 3. (**A** and **B**) Percent OT-I and P14 cells, tracked in the experiment shown in Figure 3A, that had either firmly adhered to (**A**) or transmigrated across (**B**) the capillary wall of B6-OVA kidney grafts. (**C**) Time-lapse images showing transendothelial migration of a PTx-treated OT-I cell (red) in a B6-OVA kidney graft; blood vessel is labeled in blue. (**D**–**F**) Motility parameters — median velocity (**D**), displacement (**E**), and arrest coefficients (**F**) — of untreated OT-I (n = 265), PTx-treated OT-I (n = 223), and untreated P14 (n = 68) cells imaged in B6-OVA grafts. Results are mean ± SEM. ND, not detected. *P < 0.05; **P < 0.01; ***P < 0.001. Scale bars: 10 μm.

displacements, and high arrest coefficients (Figure 4, D–F, and ref. 26). However, significant differences in the motility of the 3 cell populations were observed. Antigen-specific (OT-I) cells had lower velocities and higher arrest coefficients than antigen-nonspecific (P14) cells. Moreover, blocking $G\alpha_i$ in OT-I cells increased their velocity and reduced their arrest coefficient, but these remained significantly less motile than P14 cells (Figure 4, D–F). Together, these findings indicate that antigen-specific effector T cells firmly adhere to and transmigrate across the graft endothelium in an antigen-dependent, $G\alpha_i$-independent fashion, while antigen-nonspecific (bystander) effector T cells depend on $G\alpha_i$ to enter the graft tissue.

We next sought to determine which graft cell is responsible for presenting antigen to migrating T cells. Although it is suspected that antigen presentation in the vascular lumen is an exclusive function of endothelial cells (27), bone marrow–derived APCs such as DCs are known to extend cellular processes across endothelial and epithelial barriers in several tissues (28–30), including the kidney (M.H. Oberbarnscheidt and F.G. Lakkis, unpublished observations). We therefore used 2-photon microscopy to analyze the migration of effector OT-I cells to B6-OVA kidney grafts that lacked the MHC class I molecule H-2KB (which is required for presenting cognate OVA peptide to OT-I cells) on the endothelium, bone marrow–derived APCs, or both. As shown in Figure 5, A–C, and Supplemental Videos 4–6, H-2KB expression on graft APCs or endothelium was sufficient for the firm adhesion and transmigration of OT-I effectors. In either case, migration was slightly less than that observed when H-2KB was present on both cell types (P < 0.05 compared with data in Figure 3A), while total absence of H-2KB in the graft reduced migration to minimal levels (Figure 5A). Motility analysis revealed that antigen presentation by bone marrow–derived APCs caused a greater degree of effector T cell arrest than endothelial cells (Figure 5, D–F). This conclusion was true for total effector T cells in the graft (Figure 5, D–F) as well as for those arrested in the capillary lumen (Supplemental Figure 1).

Imaging of OT-I effectors in B6-OVA kidneys in which only bone marrow–derived APCs expressed H-2KB and DCs were genetically labeled with yellow fluorescent protein (YFP) confirmed that the majority of arrested T cells, regardless of location, made stable contacts with DCs in the graft (Figure 6A). An example of an OT-I cell arresting in the capillary lumen after contact with a DC is shown graphically (instantaneous velocity versus time) and in video and time-lapse images in Figure 6B and Supplemental Video 7. Furthermore, OT-I cells maintained contact with graft DCs throughout the transmigration process (Figure 6C and Supplemental Video 8). These findings establish bone marrow–derived graft APCs as an alternative but remarkably robust pathway by which effector T cells firmly adhere to and transmigrate across the capillary wall.

Discussion

Our findings shed new light on the pathogenesis of transplant rejection and, more broadly, the immune surveillance of nonlymphoid tissues by $CD8^+$ T cells. We established that a key step in the rejection of transplanted organs, the migration of antigen-specific effector T cells into the inflamed graft, was governed by cognate antigen and not by $G\alpha_i$-dependent chemokine signaling.

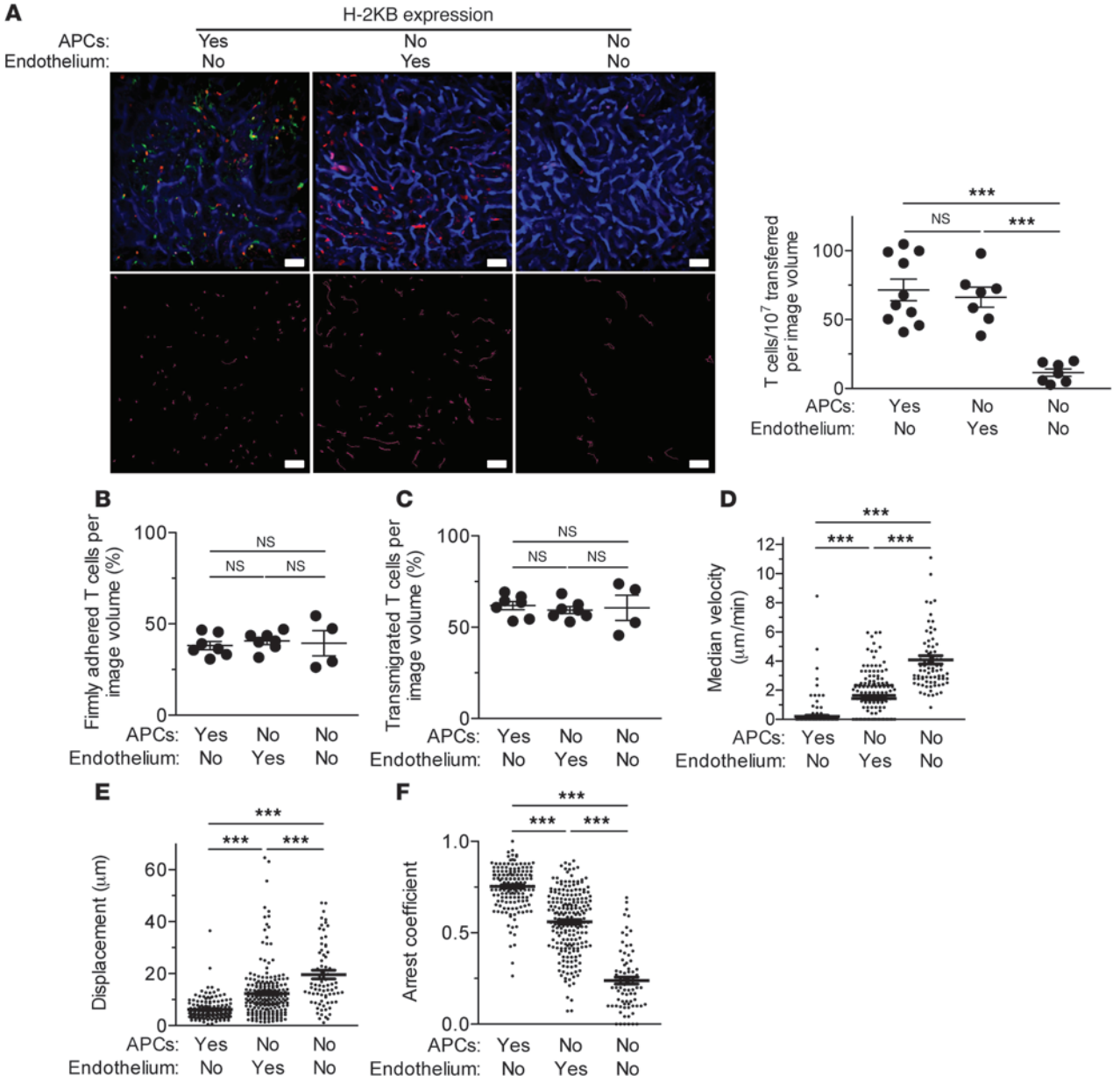

Figure 5

Presentation of cognate antigen by either graft endothelium or bone marrow–derived APCs is sufficient for the transmigration of effector T cells. OT-I effectors were imaged as described in Figure 3. (**A**) Visualization and enumeration of OT-I cells arrested in B6-OVA kidney grafts that lack H-2KB expression on the endothelium (WT CD11c-YFP$^+$→*H2kb*$^{-/-}$ chimeric graft to WT CD11c-YFP$^+$ recipient), APCs (*H2kb*$^{-/-}$→WT chimeric graft to *H2kb*$^{-/-}$ recipient), or both (*H2kb*$^{-/-}$ graft to *H2kb*$^{-/-}$ recipient) (n = 7–10 videos/group, 2–3 independent experiments). Volume-rendered representative time point images (top) show arrested OT-I cells (red); green cells (left) are YFP$^+$ DCs; blood vessels are labeled in blue. Time projections (bottom) depict OT-I cells (red) tracked over approximately 30 minutes. (**B** and **C**) Percent OT-I cells that had either firmly adhered to (**B**) or transmigrated across (**C**) the capillary wall of B6-OVA kidney grafts in the same experimental groups in **A**. (**D**–**F**) Motility parameters — median velocity (**D**), displacement (**E**), and arrest coefficients (**F**) — of OT-I cells imaged in B6-OVA kidney grafts that lack H-2KB expression on the endothelium (n = 168), APCs (n = 206), or both (n = 77). Results are mean ± SEM. ***P < 0.001. Scale bars: 50 μm.

$G\alpha_i$ signaling, however, was necessary for recruiting bystander T cells. A similar sequence of events, cognate antigen–driven migration of antigen-specific CD4$^+$ T cells followed by chemokine-dependent entry of bystander antigen-nonspecific T cells into the target tissue, has been reported in the early stages of mouse autoimmune diabetes (31, 32), which suggests that the antigen-dependent migration paradigm applies more widely to both CD4$^+$ and CD8$^+$ T cells and to different disease states. Antigen-dependent immune surveillance of nonlymphoid tissues may be advantageous to the host. By restricting the entry of effector or memory T cells to nonlymphoid sites where non–self-antigen is present, antigen-dependent T cell migration increases the effi-

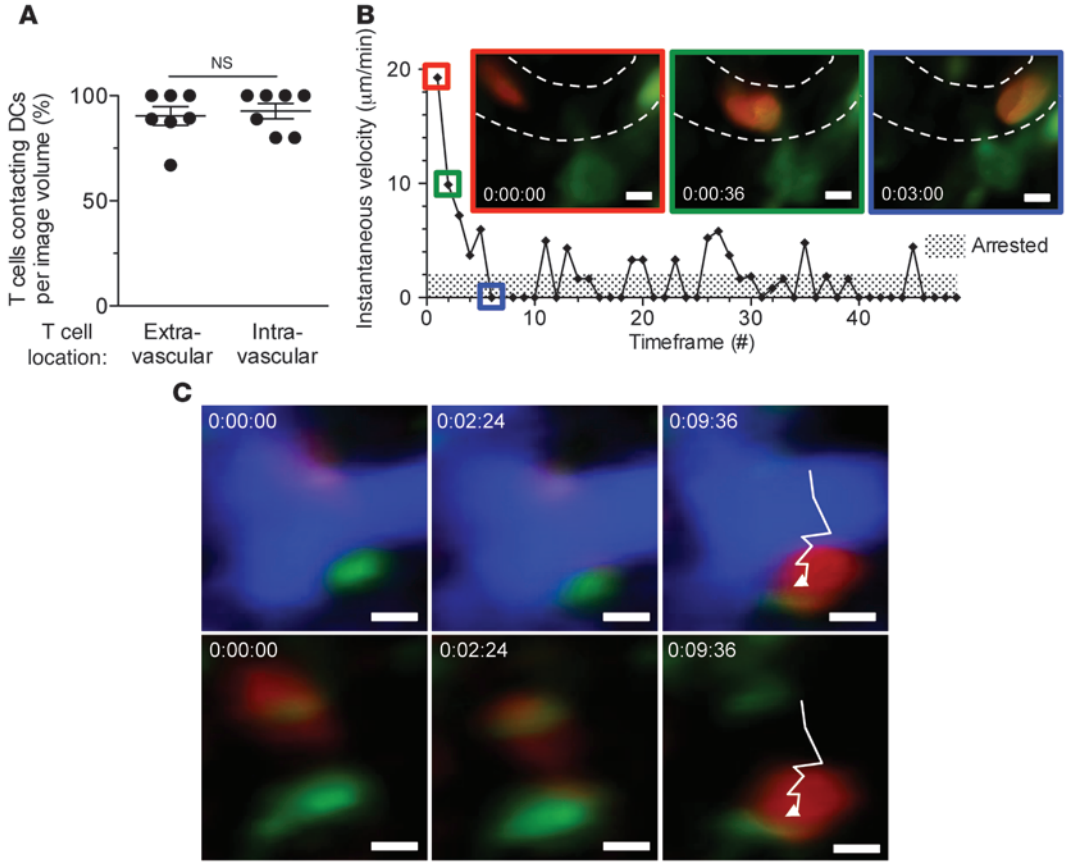

Figure 6
Effector T cell interaction with bone marrow–derived APCs during firm adhesion and transmigration. OT-I effectors were imaged as described in Figure 3. Results shown are analysis of first experimental group in Figure 5A. (**A**) Percent OT-I cells making stable contacts with YFP+ DCs in B6-OVA kidney grafts in which H-2KB expression was restricted to bone marrow–derived APCs (n = 7 videos, 3 independent experiments). (**B**) Visualization and instantaneous velocity of an OT-I cell (red) arrested in a blood vessel (dashed outline) after making stable contact with a YFP+ DC (green). (**C**) Time-lapse images showing an OT-I cell (red) making stable contact with a YFP+ DC (green) throughout the transmigration process. Blood vessel (blue) is subtracted below. Results are mean ± SEM. Scale bars: 5 μm.

ciency by which the antigen is eliminated and at the same time prevents immunopathology in tissues in which the antigen is absent. Finally, we established that antigen presentation by bone marrow–derived graft APCs was sufficient for arresting effector T cells in the capillary lumen and inducing their transmigration across the capillary wall. This previously unappreciated pathway of effector T cell entry into vascularized organ transplants sheds new light on the pathogenesis and treatment of rejection.

Methods

Mice

B6 mice (C57BL/6J; Thy1.2, CD45.2, H-2B), B6.PL-Thy1a/CyJ mice (Thy1.1, CD45.2, H-2B), BALB/cJ mice (BALB/c; H-2D), B6-OVA mice (C57BL/6J-Tg[CAG-OVA]916Jen/J; CD45.2, H-2B), OT-I mice (C57BL/6-Tg[TcraTcrb]1100Mjb/J; CD45.2, H-2B), and B6 CD11c-YFP mice were purchased from The Jackson Laboratory. P14 mice (B6.Cg-Tcra^{tm1Mom}-Tg[TcrLCMV]327Sdz; CD45.2, H-2B) and B6 *H2kb*$^{-/-}$ mice were purchased from Taconic. B6 OVA^{+}CD11c-YFP^{+} mice and OVA^{+}*H2kb*$^{-/-}$ mice were generated by cross-breeding B6-OVA mice with B6 CD11c-YFP and B6 *H2kb*$^{-/-}$ mice, respectively. B6-Ly5.2/Cr mice (Thy1.2, CD45.1, H-2B) were purchased from NCI. OT-I mice were bred onto *Rag*$^{-/-}$ Thy1.1 and *Rag*$^{-/-}$ Thy1.2 backgrounds. *aly/aly* mice (Map3k14$^{aly/aly}$; Thy1.2, H-2B) were purchased from CLEA and bred onto a B6 CD45.1 congenic background. All animals were maintained under specific pathogen–free conditions.

Surgical procedures and bone marrow chimeras

Splenectomies and heterotopic transplantation of vascularized heart and kidney grafts were performed as previously described (2, 25, 33). Heart graft rejection, defined as cessation of palpable heartbeat, was confirmed by histological analysis. Bone marrow chimeras were generated by irradiating recipient mice with 1,000 cGy from a Nordion Gamma Cell 40 cesium source. After irradiation, the mice were injected retro-orbitally with 1×10^7 donor bone marrow cells. After an 8-week reconstitution period, blood was phenotyped to verify appropriate reconstitution. Chimerism was consistently greater than 90%–95% in the blood and was confirmed in selected kidneys.

Generation, isolation, and adoptive transfer of effector and memory T cells

Polyclonal cells. Polyclonal CD4^{+} and CD8^{+} effector and memory T cells were generated as described previously (12). Briefly, B6 (CD45.2) mice on the Thy1.1 and Thy1.2 backgrounds were immunized i.p. with 2×10^7 BALB/c splenocytes on days 0 and 21. At 1 or 6–8 weeks after the first

immunization, spleen and lymph node cells were harvested to obtain effector and memory T cells, respectively; enriched for T cells by negative selection; labeled with CFSE (Invitrogen); and treated or not with 200 ng/ml PTx (Sigma-Aldrich) for 30 minutes at 37°C (5% CO_2). Subsequently, $CD44^{hi}CFSE^+$ $CD4^+$ and $CD8^+$ effector and memory T cells were sorted on a BD Aria Plus high-speed sorter (purity, ~95%). To study migration, equal numbers of PTx-treated (Thy1.1, CD45.2) and untreated (Thy1.2, CD45.2) $CD4^+$ and $CD8^+$ effector or memory T cells (2–3 × 10^6 each) were cotransferred i.v. into B6 (Thy1.2, CD45.1) or splenectomized *aly/aly* (Thy1.2, CD45.1) recipients of BALB/c heart allografts. To study allograft rejection, the same number of PTx-treated or untreated memory T cells were transferred separately into splenectomized *aly/aly* recipients.

Monoclonal (TCR transgenic) cells. DCs were generated by culturing bone marrow cells with IL-4 and GM-CSF (Peprotech) for 8 days. DCs were stimulated with 100 ng/ml LPS overnight and pulsed with either 10 μg/ml OVA (SIINFEKL) or 5 μg/ml LCMV (KAVYNFATM) peptides (Genscript) for 2 hours at 37°C. 2–3 × 10^6 OVA or LCMV peptide-pulsed DCs were injected i.v. with 5 × 10^5 OT-I (Thy1.1, CD45.2) or P14 (Thy1.2, CD45.2) T cells, respectively, into B6 (Thy1.2, CD45.1) mice based on previously published methods (34). 5 days later, spleen and lymph node cells were labeled with CFSE and treated or not with PTx, and OT-I and P14 effectors were recovered by high-speed sorting of $CD45.2^+CD8^+CFSE^+$ cells. Flow analysis confirmed that >95% of these cells were $CD44^{hi}$ and were OVA or LCMV MHCI tetramer positive (Beckman Coulter). OT-I and/or P14 effectors, with or without PTx treatment, were then cotransferred i.v. (1–2 × 10^6 each) into B6 (Thy1.2, CD45.1) recipients of either B6-OVA or B6 heart grafts. To study the role of VLA-4 in migration, OT-I effector T cells were incubated prior to transfer with 100 μg/ml monoclonal rat anti-mouse VLA-4 antibody (PS/2; BioXCell) on ice for 20 minutes. In addition, recipients received 250 μg PS/2 i.p. on the day of cell transfer as well as 1 and 2 days later. For the intravital imaging studies, cells were labeled prior to transfer with 2 μM CFSE, cell tracker orange (CTO), or cell tracker violet (CTV) (Invitrogen), then high-speed sorted by gating on $CD45.2^+CFSE^+CTO^+CTV^+$ cells, using the following dump channel: $CD4^+CD45R/B220^+CD11c^+CD11b^+CD49b^+Ly\text{-}76^+CD16/32^+F4/80^+$. Flow analysis confirmed that sorted populations were >95% $CD8^+CD44^+$ and were tetramer positive. OT-I and/or P14 effectors, with or without PTx treatment, were then cotransferred i.v. (7–10 × 10^6 each) into B6 (Thy1.2, CD45.1) recipients of B6-OVA, B6, or chimeric kidney grafts.

Analysis of cell migration by flow cytometry

Heart grafts, kidney grafts, spleen, and lymph nodes were harvested at the indicated time points after T cell transfer. Lymphocytes were isolated from heart and kidney grafts as previously described (12). Total recovered lymphocyte number was determined, and the transferred polyclonal and monoclonal T cells were enumerated by flow cytometry by gating on the $CD45.2^+Thy1.1^+$ and $CD45.2^+Thy1.2^+$ populations after live/dead cell discrimination and exclusion of non-T cells ($CD45R/B220^+CD11c^+CD11b^+CD49b^+Ly\text{-}76^+CD16/32^+F4/80^+$). Fluorochrome- or biotin-tagged antibodies (purchased from BD Pharmingen, eBioscience, Biolegend, or R&D Systems) were as follows: BDCD90.1 (clone OX-7), CD90.2 (clone 30-H12), CD45.2 (clone 104), CD45.1 (clone A20), CD8 (clone 53-6.7), CD4 (clone RM4-5), CD44 (clone IM7), CD62L (clone MEL-14), CD45R/B220 (clone RA3-6B2), CD11c (clone HL3), CD11b (clone M1/70), CD49b (clone DX5), Ly-76 (clone TER-119), CD16/32 (clone 2.4G2), and F4/80 (clone BM8). Fixable live/dead Aqua cell stain (405 nm excitation) was purchased from Invitrogen. Flow acquisition was performed on LSRII and LSRFortessa analyzers (BD Biosciences), and data were analyzed using Flowjo software (Treestar Corp.).

2-photon intravital microscopy and image analysis

2-photon intravital microscopy was performed on transplanted kidneys using a previously established method (25). An Olympus FluoView FV1000 microscope with a Mai Tai DeepSee femtosecond-pulsed laser (Spectra-Physics), tuned and mode-locked to either 825 nm or 860 nm, was used for all experiments. The recipient mouse was anesthetized with isoflurane and oxygen and placed on a heating pad to maintain core body temperature at 37°C. An i.v. line was inserted in the external jugular vein to provide 5% dextrose lactated ringer's solution for hydration and 500 kDa dextran conjugated with either FITC or rhodamine for visualization of blood vessels in the transplanted kidney. The kidney graft was extraverted from the abdominal cavity with intact vascular connection and immobilized in a custom cup mount (25). A coverslip was placed on top of the kidney, and *z* stacks were visualized with a ×25 water immersion objective (SP1, NA 1.05) 25–55 μm below the kidney capsule. 12 slices were acquired at a step size of 2.7 μm. Brightness and laser power were adjusted based on the imaging depth and kept below phototoxic levels. Dwell time was set to 8 μs/pixel, and resolution was a maximum of 512 × 512. The scanning area was cropped to adjust for a 30-second-long *z* stack that was then repeatedly scanned up to 60 times, for a maximum imaging time of 30 minutes per location. Settings were repeated in up to 5 locations per transplanted kidney. T cells were enumerated at 7 independent time points per *z* stack. All acquired videos were analyzed using Volocity software (Perkin-Elmer). Drift was corrected using the blood vessels as a reference point. Cells present in the field of view for at least 5 time points (>2 minutes) were tracked in the *x*, *y*, and *z* direction for the duration of each video. Cells were determined to have firmly adhered if they were arrested for >30 seconds in the capillary lumen, and transmigrated if most or all of the cell body had moved outside the capillary lumen at any time during the course of their tracking. Motility parameters were plotted using Volocity software.

In vitro migration assay

5-μm pore size chemotaxis assay chamber (Millipore) was used with or without 0.5 μg/ml IP-10 in medium in the bottom chamber. 5 × 10^4 OT-I effector T cells, isolated as described above, with or without PTx pretreatment were placed in the top chamber of each well for a total of 7–12 wells per group. The chamber was incubated at 37°C for 3 hours, after which the cells in the bottom chamber were collected and counted using a hemocytometer and trypan blue exclusion. The assay was repeated using OT-I effector T cells restimulated with OVA-pulsed DCs at 37°C for 2 hours prior to use in the chemotaxis assay. This restimulation protocol was sufficient to induce IFN-γ production in 60% of the cells.

Statistics

Statistical analysis of allograft survival was calculated using the log-rank test. All other experiments were analyzed using 2-tailed unpaired *t* test for samples with normal distribution and 2-tailed Mann-Whitney test for samples with non-Gaussian distribution. All statistical calculations were made using GraphPad Prism version 5.0c. A *P* value less than 0.05 was considered significant.

Study approval

All animal studies were approved by the University of Pittsburgh IACUC (protocol no. 12050385; PHS assurance no. A3187-01).

Acknowledgments

This work was supported by NIH grant AI049466 to F.G. Lakkis; NIH grant AI064343 to F.G. Lakkis, D.M. Rothstein, and W.D.

Shlomchik; and the Frank and Athena Sarris Chair in Transplantation Biology at the University of Pittsburgh. J.M. Walch was supported by NIH training grant T32 AI74490. We thank the Ferris lab (University of Pittsburgh) for technical assistance with the in vitro migration assay and the O'Brien Center for Advanced Microscopic Analysis (Indiana University) for invaluable support in establishing mouse renal imaging.

Received for publication September 4, 2012, and accepted in revised form February 21, 2013.

Address correspondence to: Fadi G. Lakkis, University of Pittsburgh, Starzl Transplantation Institute, BST W1548, 200 Lothrop Street, Pittsburgh, Pennsylvania 15261, USA. Phone: 412.383.5774; Fax: 412.383.9990; E-mail: lakkisf@upmc.edu.

1. Macedo C, et al. Contribution of naive and memory T-cell populations to the human alloimmune response. *Am J Transplant*. 2009;9(9):2057–2066.
2. Lakkis FG, Arakelov A, Konieczny BT, Inoue Y. Immunologic 'ignorance' of vascularized organ transplants in the absence of secondary lymphoid tissue. *Nat Med*. 2000;6(6):686–688.
3. Chalasani G, Dai Z, Konieczny BT, Baddoura FK, Lakkis FG. Recall and propagation of allospecific memory T cells independent of secondary lymphoid organs. *Proc Natl Acad Sci U S A*. 2002; 99(9):6175–6180.
4. Obhrai JS, Oberbarnscheidt MH, Hand TW, Diggs L, Chalasani G, Lakkis FG. Effector T cell differentiation and memory T cell maintenance outside secondary lymphoid organs. *J Immunol*. 2006; 176(7):4051–4058.
5. Schenk AD, Nozaki T, Rabant M, Valujskikh A, Fairchild RL. Donor-reactive CD8 memory T cells infiltrate cardiac allografts within 24-h posttransplant in naive recipients. *Am J Transplant*. 2008; 8(8):1652–1661.
6. Springer TA. Traffic signals for lymphocyte recirculation and leukocyte emigration: the multistep paradigm. *Cell*. 1994;76(2):301–314.
7. Shulman Z, et al. Lymphocyte crawling and transendothelial migration require chemokine triggering of high-affinity LFA-1 integrin. *Immunity*. 2009; 30(3):384–396.
8. Kitchens WH, et al. Integrin antagonists prevent costimulatory blockade-resistant transplant rejection by CD8+ memory T cells. *Am J Transplant*. 2012; 12(1):69–80.
9. Setoguchi K, Schenk AD, Ishii D, Hattori Y, Baldwin WM. LFA-1 antagonism inhibits early infiltration of endogenous memory CD8 T cells into cardiac allografts and donor-reactive T cell priming. *Am J Transplant*. 2011;11(5):923–935.
10. Hancock WW, Gao W, Faia KL, Csizmadia V. Chemokines and their receptors in allograft rejection. *Curr Opin Immunol*. 2000;12(5):511–516.
11. Halloran PF, Fairchild RL. The puzzling role of CXCR3 and its ligands in organ allograft rejection. *Am J Transplant*. 2008;8(8):1578–1579.
12. Oberbarnscheidt MH, et al. Memory T cells migrate to and reject vascularized cardiac allografts independent of the chemokine receptor CXCR3. *Transplantation*. 2011;91(8):827–832.
13. Spangrude GJ, Sacchi F, Hill HR, Van Epps DE, Daynes RA. Inhibition of lymphocyte and neutrophil chemotaxis by pertussis toxin. *J Immunol*. 1985; 135(6):4135–4143.
14. Bargatze RF, Butcher EC. Rapid G protein-regulated activation event involved in lymphocyte binding to high endothelial venules. *J Exp Med*. 1993; 178(1):367–372.
15. Warnock R, Askari S, Butcher E, von Andrian UH. Molecular mechanisms of lymphocyte homing to peripheral lymph nodes. *J Exp Med*. 1998; 187(2):205–216.
16. Savinov AY, Wong FS, Stonebraker AC, Chervonsky AV. Presentation of antigen by endothelial cells and chemoattraction are required for homing of insulin-specific CD8+ T cells. *J Exp Med*. 2003; 197(5):643–656.
17. Marelli-Berg FM, et al. Cognate recognition of the endothelium induces HY-specific CD8+ T-lymphocyte transendothelial migration (diapedesis) in vivo. *Blood*. 2004;103(8):3111–3116.
18. Galea I, Bernardes-Silva M, Forse PA, van Rooijen N, Liblau RS, Perry VH. An antigen-specific pathway for CD8 T cells across the blood-brain barrier. *J Exp Med*. 2007;204(9):2023–2030.
19. Manes TD, Pober JS. Antigen presentation by human microvascular endothelial cells triggers ICAM-1-dependent transendothelial protrusion by, and fractalkine-dependent transendothelial migration of, effector memory CD4+ T cells. *J Immunol*. 2008;180(12):8386–8392.
20. Schenk AD, Gorbacheva V, Rabant M, Fairchild RL, Valujskikh A. Effector functions of donor-reactive CD8 memory T cells are dependent on ICOS induced during division in cardiac grafts. *Am J Transplant*. 2009;9(1):64–73.
21. Dustin ML, Springer TA. T-cell receptor cross-linking transiently stimulates adhesiveness through LFA-1. *Nature*. 1989;341(6243):619–624.
22. Dustin ML, Bromley SK, Kan Z, Peterson DA, Unanue ER. Antigen receptor engagement delivers a stop signal to migrating T lymphocytes. *Proc Natl Acad Sci U S A*. 1997;94(8):3909–3913.
23. Raab M, et al. T cell receptor "inside-out" pathway via signaling module SKAP1-RapL regulates T cell motility and interactions in lymph nodes. *Immunity*. 2010;32(4):541–556.
24. Abram CL, Lowell CA. The ins and outs of leukocyte integrin signaling. *Annu Rev Immunol*. 2009; 27:339–362.
25. Camirand G, et al. Multiphoton intravital microscopy of the transplanted mouse kidney. *Am J Transplant*. 2011;11(10):2067–2074.
26. Textor J, Peixoto A, Henrickson SE, Sinn M, von Andrian UH, Westermann J. Defining the quantitative limits of intravital two-photon lymphocyte tracking. *Proc Natl Acad Sci U S A*. 2011; 108(30):12401–12406.
27. Pober JS, Tellides G. Participation of blood vessel cells in human adaptive immune responses. *Trends Immunol*. 2012;33(1):49–57.
28. Choi JH, et al. Identification of antigen-presenting dendritic cells in mouse aorta and cardiac valves. *J Exp Med*. 2009;206(3):497–505.
29. Ouchi T, et al. Langerhans cell antigen capture through tight junctions confers preemptive immunity in experimental staphylococcal scalded skin syndrome. *J Exp Med*. 2011;208(13):2607–2613.
30. Niess JH, et al. CX3CR1-mediated dendritic cell access to the intestinal lumen and bacterial clearance. *Science*. 2005;307(5707):254–258.
31. Calderon B, Carrero JA, Miller MJ, Unanue ER. Cellular and molecular events in the localization of diabetogenic T cells to islets of Langerhans. *Proc Natl Acad Sci U S A*. 2011;108(4):1561–1566.
32. Calderon B, Carrero JA, Miller MJ, Unanue ER. Entry of diabetogenic T cells into islets induces changes that lead to amplification of the cellular response. *Proc Natl Acad Sci U S A*. 2011;108(4):1567–1572.
33. Corry RJ, Winn HJ, Russel PS. Primarily vascularized allografts of hearts in mice: The role of H-2D, H-2K, and non H-2 antigens. *Transplantation*. 1973; 16(4):343–350.
34. Badovinac VP, Messingham KAN, Jabbari A, Haring JS, Harty JT. Accelerated CD8+ T-cell memory and prime-boost response after dendritic-cell vaccination. *Nat Med*. 2005;11(7):748–756.